JOURNAL OF GEOPHYSICAL RESEARCH, VOL. 103, NO. C5, PAGES 10,451–10,468, MAY 15, 1998

A statistical comparison of wind speed, wave height, and wave period derived from satellite altimeters and ocean buoys in the Gulf of Mexico region

Paul A. Hwang, William J. Teague, and Gregg A. Jacobs

Oceanography Division, Naval Research Laboratory, Stennis Space Center, Mississippi

David W. Wang

Computer Science Corporation, Stennis Space Center, Mississippi

Abstract. The capability of spaceborne altimeters to provide precise measurement of significant wave height and wind speed has been demonstrated repeatedly. It is shown in this paper that in addition to the significant wave height and wind speed, the wave period can be calculated from the semiempirical functions established from earlier wave research. The calculated characteristic wave period using the altimeter-derived wind speed and wave height are found to be in excellent agreement with the peak wave period and average wave period from the ocean buoy measurements in the Gulf of Mexico. Also, with the long time series of collocated data set, it is possible to compare altimeter output of wind and wave parameters with ocean buoy measurements taking into consideration the spatial lags between the buoy locations and the altimeter footprints, and the temporal lags between the two sensor systems. It is found that when the spatial lags are less than 10 km, the RMS difference of the significant wave height is approximately 0.1 m, which is the digitization resolution of the output from both altimeter and ocean buoy. For the wind speed, the RMS difference approaches 1.2 m/s in the Gulf of Mexico using the empirical algorithms. The wind speed agreement is significantly improved to 0.8 m/s when the tilting effect on the altimeter cross section is accounted for. In contrast to the spatial lags, temporal lags of up to 1 hour do not appear to produce significant difference in the statistics of comparison based on this study.

1. Introduction

Satellite remote sensing provides an efficient way for monitoring global and regional oceanographic parameters. Spaceborne altimeters following their many generations of development have provided high-quality data on the sea state with an unusually high spatial density. For example, TOPEX/POSEIDON (hereinafter referred to as TOPEX) provides wind and wave information every second, corresponding to approximately a 7-km resolution along the satellite tracks. The spacing of the tracks is nominally 316 km (127 revolutions per repeat cycle) at the equator and much smaller at higher latitudes. The revisiting period of each track is 9.9156 days [*Fu et al.*, 1994]. With such a high density coverage we can study the regional wave climatology using the TOPEX altimeter output of wind and wave parameters [*Teague et al.*, 1997].

The TOPEX geophysical data record includes the significant wave height and normalized radar cross section, which can be used to calculate the wind speed. The significant wave height is derived from the average wave form of radar returns. For the TOPEX mission, the altimeter sends out 4000 pulses per second [*Chelton et al.*, 1989]. The wave height and radar cross section reported every second therefore represent the averages of 4000 samples. These measurements are the basis for deriving the wind and wave parameters from satellite altimeters. Section 2 describes the comparison of significant wave height from the Ku and C band altimeters with in situ measurements. The dependence of the RMS difference and the correlation coefficient on the spatial distance between the satellite footprint and the buoy location is calculated. Similarly, the dependence of the statistics on the time lags between the remote sensing and in situ measurements is presented. The same procedure of wave height comparison is applied to the wind speed parameter using the Ku band radar cross section and is discussed in section 3. In addition to the processing of spatial and temporal lags, this section also describes the tilting effect (caused by water waves that are much longer than the radar waves) on the altimeter backscattering. The effect introduces a strong attenuation of the radar backscattering cross section. It is shown that when this tilting effect is accounted for, the agreement of the wind speed derived from the altimeter with the buoy measurement is significantly improved.

Since the wave height, wind speed, and wave period are closely related as we have learned from extensive ocean wave studies through the years [e.g., *Hasselmann et al.*, 1973, 1976; *Toba*, 1978], the correlations established from those studies are applied to the TOPEX data to retrieve a characteristic wave period from the wave height and wind speed output. The obtained characteristic wave period is shown to be closely related to the peak wave period or the average wave period obtained from buoy measurements in the Gulf of Mexico. The details are provided in section 4. It is therefore possible to derive the three most critical parameters of a wave field, the significant wave height, characteristic wave period, and wind speed, from the satellite altimeters. The summary and conclusions are given in section 5.

Paper number 98JC00197.
0148-0227/98/98JC-00197$09.00

2. Significant Wave Height

2.1. Overview

Comparisons of TOPEX significant wave heights (H_S) with in situ measurements from surface buoys have shown very positive agreement [e.g., *Ebuchi and Kawamura*, 1994; *Gower*, 1996]. In particular, Gower [1996] presents a comprehensive comparison of wind speed and wave height between the TOPEX altimeter measurement and 14 moored buoys along the west coast of Canada, of which three are in the open ocean, approximately 400 km west of the British Columbia coast, six are in the exposed positions within 100 km from the coast, and five are in sheltered coastal waters. He performed detailed statistical comparisons of these three groups of buoys with all three altimeters (NASA (National Aeronautics and Space Administration) Ku and C band altimeters and CNES (Centre National d'Etudes Spatiales) Ku band solid state altimeter). The temporal difference between TOPEX and buoy measurements is less than 30 min, and the spatial distance is less than 107 km. An excellent agreement between the altimeter and buoy measurements of the significant wave height is found for the nine buoys in exposed positions. From the Ku band data the fitted slope of the scatterplots is 0.94 for the three outer buoys and is 0.98 for the six inner buoys. The RMS differences are 0.35 and 0.30 m, respectively, for these two data groups. For coastal regions, the agreement is clearly deteriorated, with fitted slopes ranging from 0.85 to 1.33, and RMS differences ranging from 0.24 to 0.60 m. The large variation in the coastal comparison is attributed to the local variation of the wave conditions due to the close proximity to the shoreline. *Gower* [1996] further shows that in the exposed locations, the RMS data scatter is greatly reduced when the spatial distance between TOPEX and buoy observations is reduced to 10 km. For the three outer buoys, it reduces from 0.35 to 0.14 m, and for the 6 inner buoys, it reduces from 0.30 to 0.15 m. The fitted slopes also improved, from 0.94 to 0.97, and 0.98 to 1.00 for the outer and inner groups, respectively. From these results, we may conclude that the output of significant wave height from the TOPEX altimeter, at 1336 km above ocean, is essentially identical to the surface buoy observation.

2.2. Gulf of Mexico Data Sets

The excellent agreement on the wave height measurement is also confirmed in the Gulf of Mexico stations. The comparison with five buoys in the Gulf of Mexico is presented in the following. The locations of the buoys and the TOPEX tracks are shown in Figure 1. Table 1 lists the properties of the data sets, including the buoy station number, coordinates, water depth, TOPEX track number, the number of data points in each data set, minimum and mean distance between the buoy and altimeter footprints (the maximum distance is fixed at 50 km), and the mean and standard deviation of the significant wave height and neutral wind speed at 10 m elevation, processed using the Liu-Katsaros-Businger (LKB) algorithm [*Liu et al.*, 1979]. The naming convention of the data set is TnnnBmmm, where nnn is the TOPEX track number, and mmm is the shortened buoy number (the second and the last two digits of the National Data Buoy Center (NDBC) five-digit designation). The comparison period covers the duration from October 1992 to December 1995, or 3.15 years.

Because surface buoy collects wave data at every hour, for each TOPEX data point, both buoy data points before and after the TOPEX time are selected for comparison. The wind and wave data from NDBC buoys are acquired and reported hourly. The significant wave height and peak wave period are derived from the buoy heave motion spectrum measured over a 20-min acquisition period starting at 30 min after the hour. The wind speed and wind direction are collected by a wind sensor located on the buoy's mast. The elevation of the wind sensor is 5 m above sea level. The wind speed and wind direction are the averages over the 8-min acquisition period starting at 42 min after the hour. For the comparison to the TOPEX data acquisition time, the representative data acquisition time for the hourly buoy wind and wave data is assigned at 40 min after the previous hour (that is,

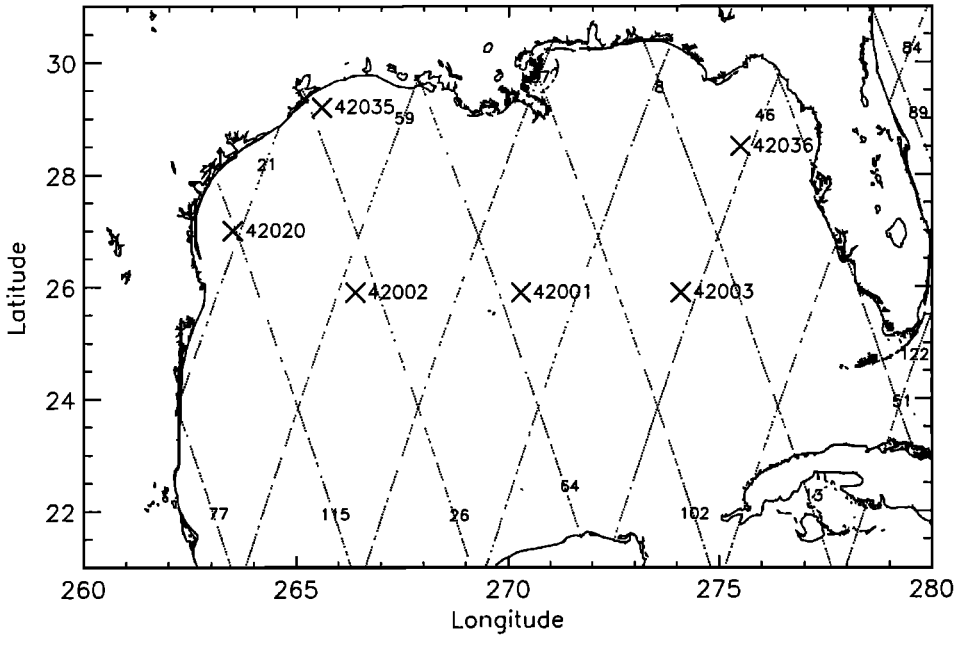

Figure 1. A map of the Gulf of Mexico and locations of buoys close to TOPEX tracks. The coordinates and the local water depths of the buoys are listed in Table 1.

Table 1. Buoy Stations and Satellite Tracks in the Gulf of Mexico Used for This Study

Data Set	Buoy Station	Buoy Location	Water Depth, m	TOPEX Track	Number of Data Points	Minimum Distance, km	Mean Distance, km	$\langle H \rangle$, m	$\langle U_{10} \rangle$, m/s	σ_H, m	σ_U, m/s
A26B202	42002	25°53'30" N 93°34'03" W	3200	26	568	45.7	47.5	1.31	6.18	0.67	2.75
A59B202				59	968	37.0	42.1	1.28	6.55	0.75	3.17
A46B203	42003	25°56'10" N 85°54'51" W	3164	46	970	38.4	42.9	1.11	6.05	0.85	3.08
A115B220	42020*	27°00'44" N 96°30'20" W	131	115	1331	5.5	26.0	1.25	6.34	0.53	2.30
A21B220				21	1286	15.8	30.0	1.42	7.10	0.69	2.92
A26B235	42035	29°14'47" N 94°24'35" W	16	26	355	26.3	36.2	0.83	5.70	0.41	2.75
A46B236	42036	28°30'01" N 84°30'08" W	51	46	879	22.6	33.6	0.94	5.53	0.79	3.10

*The location of buoy 42020 before November 30, 1993, was 27°00'18" N, 96°29'56" W.

the acquisition time is 10:40 for the buoy report time 11:00). The comparison time is therefore at the middle of the wave data acquisition period, and 6 min before the mid-point of the wind record. The buoy data points are separated into two groups. The time lags (TOPEX acquisition time minus buoy acquisition time) of the first group are less than 0.5 hour, with an average (T_1) close to 0.25 hour. The time lags for the second group are greater than 0.5 but less than 1 hour, with an average (T_2) approximately 0.75 hour (Table 2).

The agreement between the altimeter and buoy measurements of most of the data sets compiled is excellent, except for the coastal station (buoy 42035). Figure 2 shows an example of the scatter plot of the Ku and C band measurements compared with buoy data of group 1 and group 2 time lags. Both NDBC and TOPEX report wave height to the resolution of 0.1 m. The coarse digitization caused many overlaps in the plotted figures. For example, the 1331 data points in data set A115B220 results in less than 80 discrete data pairs. To reflect the density of data on each plotted point in the figure, the size of the plotting symbol is adjusted to be proportional to the number of data points falling in the same plotting coordinates. More objectively, key statistical parameters are calculated and listed in Table 2 for each data set. These parameters include the proportionality (regression) coefficient, that is, the slope for the linear regression fitting with the intercept forced to zero (*slope0*), the bias (TOPEX minus buoy), the slope (*slope1*) and intercept (*intercept1*) of the least squares linear fitting, the RMS difference, and the correlation coefficient between the altimeter and buoy measurements.

Two different estimates of *slope0* are listed. The first number corresponding to the one from minimizing the mean square difference in the y direction for a fitting of $y=(slope0)x$. The second (in parentheses) is the symmetric regression coefficient, which takes into account the fact that there are inherent errors in both sets of measurements used in the fitting (TOPEX wave height and Buoy wave height in this case). A more detailed description of the linear regression coefficients is given by *Bauer et al.* [1992], who present the formulae for four different linear regression coefficients with the intercept forced to the origin. Two of the formulae yield the coefficients of symmetric regression, the formula for minimizing the orthogonal distances of the data points to the regression line was not used because it has singularity at $y=x$ and becomes very sensitive when the regression coefficient is close to unity. A brief summary of the four regression coefficients described by *Bauer et al.* [1992] is given in the Appendix.

These statistical coefficients are presented for the two altimeter frequencies and two time lag groups. The notation in the first column of Table 2 is the combination of the frequency band (Ku or C) and the time lag group (1 or 2). For example, for the data set A115B220 (TOPEX track 115, NDBC buoy 42020), the *slope0* are 0.96 (0.96), 0.97 (0.97), 0.98 (1.00), and 0.99 (1.01), the RMS differences are 0.15, 0.15, 0.18, and 0.18 m, and the correlation coefficients are 0.96, 0.96, 0.94 and 0.94 for Ku band group 1 (time lags less than 0.5 hour), Ku band group 2 (time lags between 0.5 to 1 hour), C band group 1 and C band group 2, respectively. The bias of the two measurements are quite small, of the order of 0.05 m. The regression slopes are close to unity when forced fitting to the origin (representing the proportionality of the two measurements). The linear best fit regression with a nonzero intercept shows consistently a positive intercept and a slope less than unity. This indicates that the TOPEX altimeters measure slightly higher waves for low sea state and slightly lower

Table 2. Summary of the Comparison Statistics Between TOPEX and in Situ Measurements of the Significant Wave Height

	Slope0	Bias, m	*Slope1*	*Intercept1*	RMS, σ_H, m	Correlation Coefficient, R
Data set A115B220, Mean Distance 26.0 km, Minimum Distance 5.5 km, Total Data Points 1331, T_1=0.26 hour, T_2=0.74 hour.						
Ku1	0.96 (0.96)	-0.03	0.86	0.15	0.153	0.96
Ku2	0.97 (0.97)	-0.02	0.88	0.13	0.146	0.96
C1	0.98 (1.00)	0.01	0.84	0.22	0.224	0.91
C2	0.99 (1.01)	0.02	0.85	0.20	0.220	0.91
Data set A21B220, Mean Distance 30.0 km, Minimum Distance 15.8 km, Total Data Points 1286, T_1=0.27 hour; T_2=0.73 hour.						
Ku1	0.94 (0.95)	-0.06	0.85	0.16	0.219	0.96
Ku2	0.94 (0.95)	-0.06	0.88	0.12	0.211	0.96
C1	0.96 (0.97)	-0.02	0.87	0.17	0.208	0.96
C2	0.96 (0.97)	-0.03	0.89	0.13	0.199	0.96
Data set A46B236, Mean Distance 33.6 km, Minimum Distance 22.6 km, Total Data Points 879, T_1=0.26 hour; T_2=0.81 hour.						
Ku1	0.91 (0.92)	-0.04	0.83	0.15	0.200	0.98
Ku2	0.95 (0.95)	-0.02	0.87	0.12	0.182	0.98
C1	0.93 (0.95)	0.00	0.81	0.20	0.221	0.97
C2	0.97 (0.98)	0.02	0.85	0.18	0.203	0.97
Data set A59B202, Mean Distance 42.1 km, Minimum Distance 37.0 km, Total Data Points 968, T_1=0.26 hour; T_2=0.75 hour.						
Ku1	0.97 (0.98)	0.01	0.88	0.18	0.189	0.97
Ku2	1.00 (1.00)	0.03	0.90	0.16	0.185	0.97
C1	0.99 (1.00)	0.05	0.86	0.23	0.220	0.96
C2	1.01 (1.02)	0.07	0.89	0.21	0.217	0.96
Data set A46B203, Mean Distance 42.9 km, Minimum Distance 38.4 km, Total Data Points 970, T_1=0.27 hour; T_2=0.77 hour.						
Ku1	0.98 (1.00)	0.05	0.86	0.20	0.240	0.96
Ku2	0.96 (0.97)	0.03	0.83	0.23	0.243	0.97
C1	1.00 (1.02)	0.08	0.86	0.24	0.265	0.96
C2	0.97 (0.99)	0.07	0.83	0.26	0.262	0.96
Data set A26B202, Mean Distance 47.5 km, Minimum Distance 45.7 km, Total Data Points 568, T_1=0.27 hour; T_2=0.73 hour.						
Ku1	0.99 (0.99)	0.01	0.91	0.13	0.165	0.97
Ku2	0.97 (0.98)	-0.02	0.91	0.10	0.176	0.97
C1	1.01 (1.02)	0.05	0.92	0.15	0.205	0.96
C2	0.99 (1.00)	0.02	0.92	0.12	0.221	0.95
Data set A26B235, Mean Distance 36.2 km, Minimum Distance 26.2 km, Total Data Points 355, T_1=0.30 hour; T_2=0.80 hour.						
Ku1	1.22 (1.26)	0.22	1.01	0.22	0.368	0.82
Ku2	1.23 (1.27)	0.22	1.03	0.20	0.371	0.82
C1	1.31 (1.85)	0.44	0.96	0.37	0.579	0.64
C2	1.32 (1.86)	0.44	0.98	0.35	0.582	0.64

for high sea state as compared to the buoy data. The last two columns of the table, the RMS difference and the correlation coefficient, are the key indicators of data agreement used in this paper and will be discussed in more details in the following.

As shown in Table 2, very high correlation between the altimeter data and surface measurements is found for most of the stations except for buoy 42035 which is very close to the shore (approximately 30 km from the nearest land). Although we have excluded TOPEX data points where the land flag is set, the side lobe effect on some of the radar points may be important. Also, the change in bathymetry for the nearshore station is relatively large, and the wave conditions within the 50 km radius may have considerable variability. Similar disagreement was found in the nearshore stations compared by *Gower* [1996] as discussed earlier. The buoy 42035 is excluded for further comparison in the following.

In general, Ku band agreement is better than C band and both altimeters produce very good quality measurements of the significant wave height. The correlation coefficients of all six data sets are higher than 0.94 (Table 2). Interestingly, the difference of agreement between the two time lag groups is quite minor. In fact, the RMS values of the Ku band data show a slight decrease in the second group in the first four cases (out of six excluding the coastal station) listed in Table 2, but the difference is not significant. There is an apparent trend of increasing RMS difference (σ_H) with increasing average distance between the satellite footprints and the buoy locations (Figure 3a and 3b), especially in the C band data. In this comparison, wave data from different locations are combined together, the results may be affected by the inherent differences of the wave conditions in the databases. It is not clear how to remove these inherent differences when combining different data sets, simple normalization schemes such as taking the ratio of the RMS difference and the average height (listed in Table 1) do not appear to be effective (Figures 3c and 3d). With 3.15 years of data, the effect of spatial and temporal lags on the agreement between TOPEX and buoy data can be assessed more consistently using the same data set, the details will be reported in the next section.

2.3. Spatial and Temporal Lags

Of the buoy stations investigated, the one closest to a TOPEX track (115) is buoy 42020 (27.005°N, 96.499°W before November 30, 1993; 27.012°N, 96.506°W after November 30, 1993).

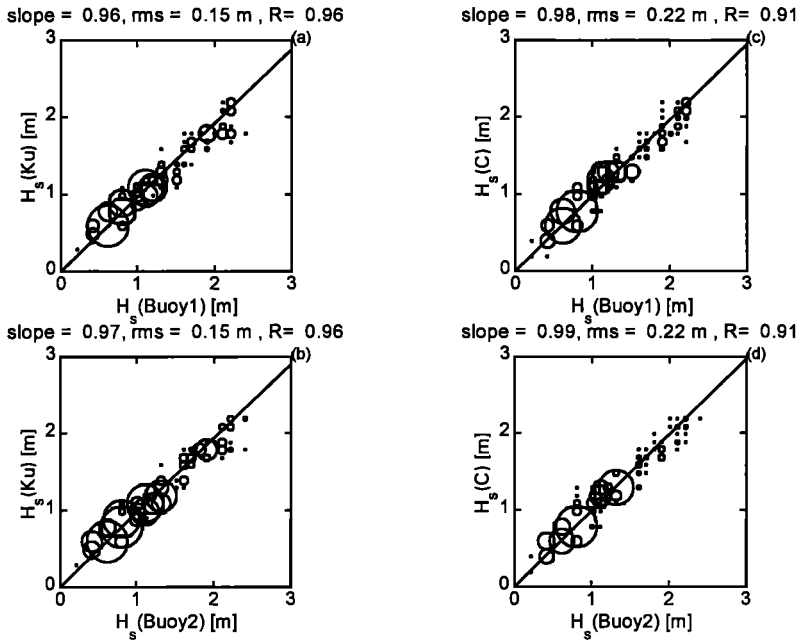

Figure 2. Scatterplot of the significant wave height measured by TOPEX altimeters and NDBC buoy (data set A115B220). (a) Ku band, time lag group 1 (less than 0.5 hour), (b) Ku band, time lag group 2 (between 0.5 to 1 hour), (c) C band, time lag group 1, and (d) C band, time lag group 2. The size of the plotting symbol is proportional to the data density.

The data set is A115B220 and has the minimal separation distance of 5.5 km. The second closest is the same buoy but with TOPEX track 21 (data set A21B220). These two data sets are used to study the effects of the spatial and temporal lags on the correlation between buoy data and TOPEX output. From October 1992 to September 1996 the total data points obtained within 50 km from the buoy are 1331 and 1286 for A115B220 and A21B220, respectively. For a few applications in the following sections, a subset of A115B220 with spatial lags less than 10 km will be referenced as T115B220. The subset contains 208 data points. For the investigation of the space lag, the data are sorted by the distance between the buoy and altimeter footprints. The typical calculation procedure divides the lags into 10 bins. The maximum space lag is 50 km, and the minimum space lag is data set dependent. The correlation coefficient and the RMS difference are then computed for each binned subset of a given space lag. The similar procedure is applied to the time lags (defined as TOPEX time minus buoy time of the measurements). Because the

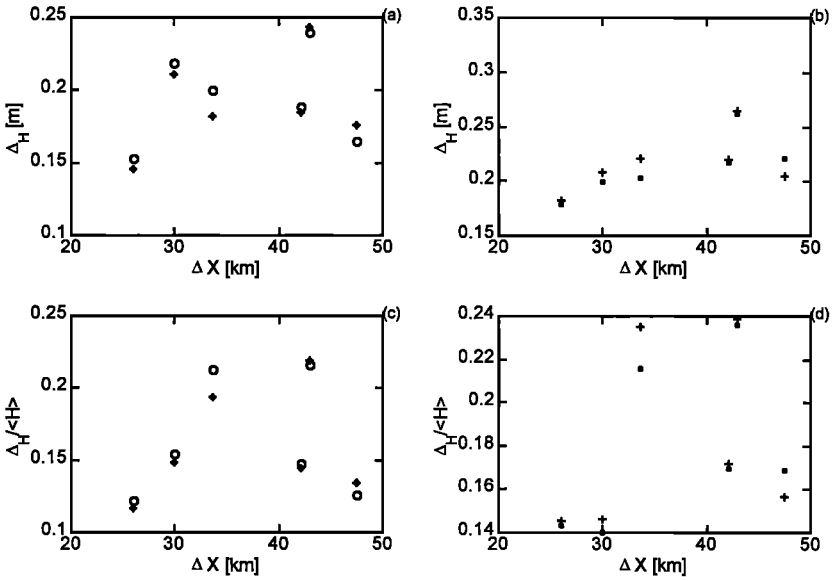

Figure 3. The dependence of the RMS difference of the significant wave height as a function of the spatial distance between buoy locations and altimeter footprints using the combined data sets listed in Table 1. Symbols used are open circles, Ku band, time lag group 1; asterisks, Ku band, time lag group 2; crosses, C band, time lag group 1; and pluses, C band, time lag group 2.

maximum time lag was chosen as 1 hour, the time lag range is from −1 to +1 hour. The correlation coefficient as a function of space lags between TOPEX and buoy measurements are shown in Figure 4a, and as a function of time lags in Figure 4b for the data set A115B220. The corresponding results for the data set A21B220 are shown in Figures 5a and 5b.

There is a general trend of reducing correlation as the spatial lag increases. For the Ku band the correlation coefficient remains quite high, ranging from 0.95 to 0.97 for A115B220 and 0.94 to 0.98 for A21B220, over the full range of the spatial lags (<50 km) investigated. The difference in the spatial correlation coefficients between the two time lag groups is minor. Interestingly, it is not unusual to find cases with higher spatial correlation in time lag group 2 than in time lag group 1, that is, a shorter time lag does not guarantee a better agreement. This result is further confirmed in the calculation of time lag dependence to be discussed below. For the C band data the spatial correlation coefficients are slightly lower than those of the Ku band, ranging from 0.91 to 0.96 for A115B220 and 0.94 to 0.97 for A21B220 (Figures. 4a and 5a). Again, the difference between the two time lag groups is minor.

The correlation coefficient as a function of time lags is not monotonic and does not have a clear trend (Figures 4b and 5b). The higher correlation coefficients usually occur at time lags significantly different from zero and may partially explain the higher spatial correlation in the time lag group 2 described earlier. Similar to the dependence on the spatial lags, the Ku band correlation coefficients (0.95 to 0.98 for group 1, 0.94 to 0.98 for group 2) are slightly higher than those of the C band (0.93 to 0.96 for group 1, 0.94 to 0.97 for group 2).

The RMS differences as functions of space lags and of time lags are shown in Figures 4c and 4d for A115B220 and in Figures 5c and 5d for A21B220. The general trend of increasing RMS difference with increasing spatial separation is in agreement with the expected decorrelation between the satellite measurements and buoy data as the distance between the satellite footprint and the buoy station increases. In contrast, the trend of the RMS difference with temporal lag is rather weak (Figures 4d and 5d). This result is consistent with the correlation computations shown in Figures 4b and 5b. In general, the trend of decorrelation with respect to spatial lags is more monotonic than the decorrelation with respect to temporal lags.

The weak dependence of the correlation on time lags is somewhat surprising. This analysis suggests that when making intercomparisons of remote sensing data and in situ measurements of the surface wave height, close proximity is more important than simultaneity of data acquisition. Note that the above statistics are derived from relatively large sample populations (1331 and 1286 points). The minimum numbers of samples per time lag bin are 186 (A115B220) and 192 (A21B220), and the minimum numbers per space lag bin are 115 (A115B220) and 91 (A21B220). Extrapolating the RMS results to the zero space lag, the RMS difference between the TOPEX and surface buoy measurements is expected to be less than 0.1 m, with a correlation coefficient of the order of 0.98. Although our present analysis is based on the data sets localized in the Gulf of Mexico, these statistics are consistent with the analyses of *Gower* [1996] who compared with buoys distributed in a much broader region in the Pacific Ocean (see Section 2.1). Such agreement from a sensor more than 1300 km above the Earth is truly amazing.

3. Wind Speed

3.1. Tilting Effect on the Altimeter Backscattering

The derivation of wind speed from microwave radars is based on the correlation of surface roughness and radar backscattering intensity (the normalized radar backscattering cross section σ_0). For the spaceborne altimeters, specular reflection is the primary mechanism of radar backscatter. In this mode, roughness on the surface causes incident waves to diffuse and scatter away from the aperture of radar reception, and the rougher the surface the less backscattering cross section is expected. On the ocean surface, short ocean waves are the primary contributor to the surface

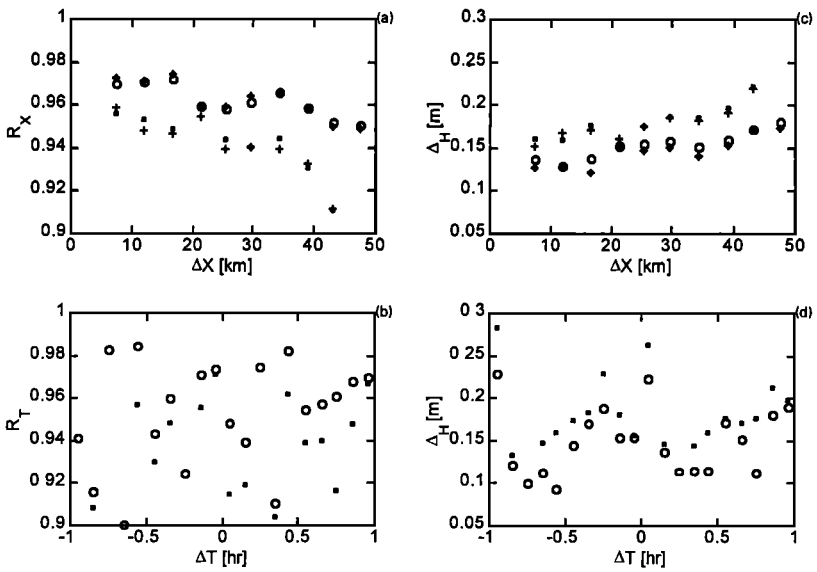

Figure 4. (a, b) The correlation coefficient and (c, d) RMS difference of wave height measurements as functions of space lag and time lag (data set A115B220). Symbols used in Figures 4a and 4b are circles, Ku band, time lag group 1; asterisks, Ku band, time lag group 2; crosses, C band, time lag group 1;, and pluses, C band, time lag group 2. Symbols used in 4c and 4d are circles, Ku band and crosses, C band.

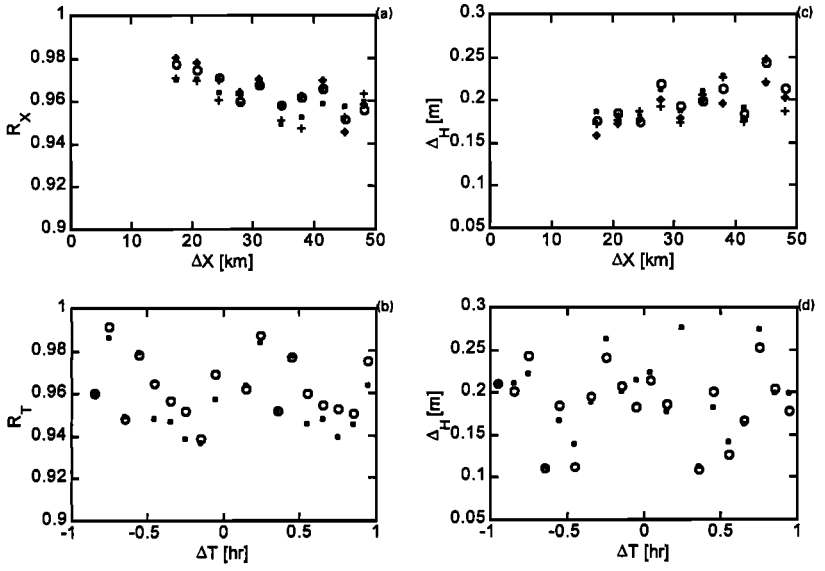

Figure 5. The correlation coefficient and RMS difference of wave height measurements as functions of space lag and time lag (data set A21B220). Symbols used are described in Figure 4.

roughness. Because these short water waves are wind generated, a higher σ_0 corresponds to a lower wind speed and vice versa. Over the past two decades, however, the operational algorithms to retrieve wind speed from the altimeter backscattering cross section have been based on empirical formulae. These formulae are either established on collocated databases of altimeter and surface in situ measurements [e.g., *Brown et al.*, 1981; *Chelton and Wentz*, 1986; *Witter and Chelton*, 1991] or based on the statistical distributions of wind speed and σ_0 separately [*Freilich and Challenor*, 1994]. Many comparisons of various algorithms [e.g., *Witter and Chelton*, 1991; *Wu*, 1992; *Freilich and Challenor*, 1994] have shown that despite the continuous improvement of the altimeter hardware and software, the progress of wind speed retrieval from various algorithms developed over the last 20 years remains stagnant. For example, *Freilich and Challenor* [1994] report a very comprehensive analysis of eight algorithms. Results in terms of the mean error, root mean square error, standard deviation, wind speed error trend and pseudo wave age error trend are tabulated. The differences in all eight algorithms are relatively minor. In terms of the mean square error and standard deviations, seven of the eight algorithms produced less than 10% differences in these two key parameters (1.60 to 1.75 m/s RMS difference, 1.58 to 1.72 m/s standard deviation).

Recently, *Hwang* [1997] presents a review of the mean square slopes derived from the ocean environment. It is shown that when comparing the mean square surface slopes derived from altimeters and the earlier in situ measurements derived from optical sensors (Figure 6a), the radar-derived mean square slopes persistently exceed the optically measured quantities for the same wind speed (Figure 6b). This is a rather unreasonable result, as the radar wavelength is a few orders of magnitude longer than the optical wavelength, therefore the radar responds to only a smaller fraction of the total roughness (low-passed by the wavelength) as compared to optical sensors. In other words, the same surface (for a given wind speed) should appear smoother to the radar than to the optical instrument, which is opposite to the results shown in Figure 6b. There are suggestions that the diffraction of small-scale waves much shorter than the radar wavelength may contribute to the attenuation of radar backscattering, thus the appearance of a rougher surface derived from the radar [e.g., *Brown*, 1978; *Jackson et al.*, 1992]. The diffraction correction may lower the altimeter-derived mean square slopes at higher wind speeds to be below the optical measurements, but the improvement at the low-wind speed range is limited [e.g., *Jackson et al.*, 1992, Figure 4]. This is because the diffraction effect relies on the presence of waves much shorter than the radar wavelength. As this portion of the short waves increases monotonically with the wind speed [*Hwang et al.*, 1996; *Hwang*, 1997], the diffraction correction will be greater in the high wind speed and less effective under low wind conditions. However, as illustrated in Figure 6b, the range of low wind speeds is where the major discrepancy between the radar and optical measurements of mean square slopes are found. The increasing difference between the radar and optical measurements toward the low wind speeds is opposite to the correction due to the diffraction effect.

Hwang et al. [1997a, b] suggest a different mechanism that contributes to the overestimate of the sea surface roughness by satellite altimeters. Through examining the zeroth order solution relating the backscattering cross section and the sea surface roughness [e.g., *Barrick*, 1968; *Brown*, 1978] given by

$$\sigma_o(\theta_i) = \frac{|R(0)|^2}{s_f^2} \sec^4\theta_i \exp\left(\frac{-\tan^2\theta_i}{s_f^2}\right), \qquad (1)$$

where θ_i is the radar incidence angle, denoting the angle between the propagation direction of radar waves and the surface normal; $|R(0)|^2$ is the Fresnel reflection coefficient, characterizing the surface reflectivity; and s_f^2 is the filtered mean square slope, representing the portion of surface roughness elements with length scales greater than the diffraction limit. Equation (1) reduces to

$$\sigma_o(0) = \frac{|R(0)|^2}{s_f^2} \qquad (2)$$

for the normal incidence condition. *Hwang et al.* [1997a, b] consider the tilting effect of longer waves that modifies the local incident angle. This is illustrated graphically in Figure 7 to describe

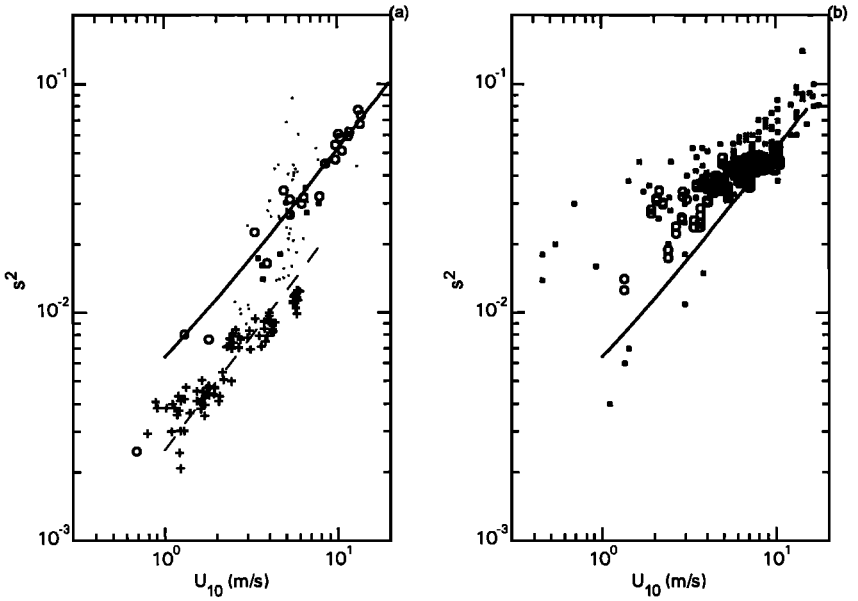

Figure 6. (a) The optically measured mean square slopes of the ocean surface as a function of wind speed. Data used are by *Cox and Munk* [1954], open circles; *Hughes et al.* [1977], crosses; *Tang and Shemdin* [1983] and *Hwang and Shemdin* [1988], solid circles, wave follower; *Hwang et al.* [1996], pluses, capillary-gravity wave components between $100<k<1600$ rad/m; the solid curve is equation (6); the dashed curve is $0.0025\ U_{10}$, fitting to the capillary-gravity wave data. (b) Ku band altimeter-derived mean square slopes. Crosses, GEOS 3 [*Brown*, 1990], open circles, TOPEX data reported in this article (data set T115B220), and the solid curve is (6) representing the average of the optical measurements.

the situation of radar waves scattering from an undulating surface with different (tilting and filtered) roughness properties and the resulting intensity patterns of the scattered waves. The sketch illustrates a train of plane waves (indicated by the parallel wave fronts), corresponding to the far-field radar waves from satellite altimeters impinging on the water surface. The scattered wave patterns from the water surface will vary according to the surface roughness conditions, being more directional and narrowly distributed from a smooth surface, as in patch 1. The primary direction of the scattering pattern is along the direction of specular reflection. Therefore, for surfaces of equivalent roughness, such as patches 2, 3, and 4, the scattering patterns are similar in the directional distribution (that is, the beam width is determined by the surface roughness), but the primary direction of the scattering will vary depending on the orientation of the roughness patch. The backscattering intensities, that is, the scattering in the direction opposite to the incoming waves, for the three patches shown will be different. The modification results in a reduced, or attenuated, radar return compared to the condition when the scattering is assumed to be on a flat surface such as depicted in patch 5. As seen from (1), the introduction of a local incident angle will produce an exponential decay in the radar cross section. This exponential decay is most significant at lower wind speeds, under which the filtered mean square slope, s_f^2, is small, and less severe

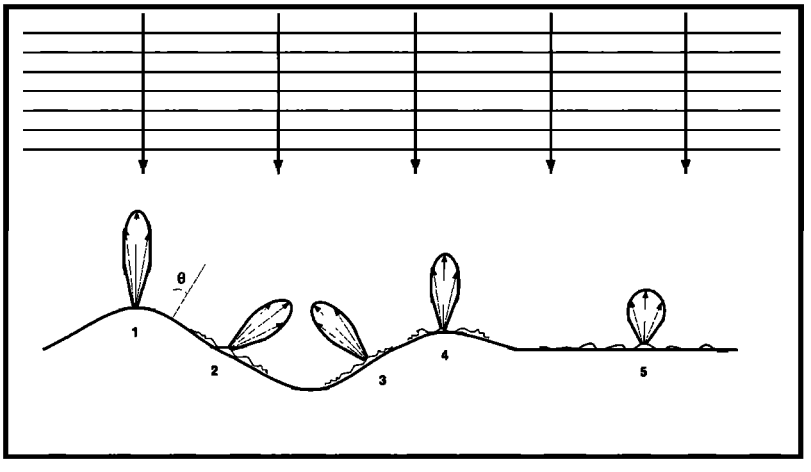

Figure 7. A conceptual sketch depicting the scattering of radar waves by surface roughness of various characteristics and the effect of tilting surface on the backscattering intensity from patches of similar roughness. See text for further description [*Hwang et al.*, 1997a].

at higher wind with $s_f^2 >> \tan^2\theta_i$. The trend of this decay due to the local incidence angle variation is in agreement with the wind-dependent anomaly in the apparent surface roughness due to the attenuation of the radar return, as shown in Figure 6b. It is concluded that the computation of σ_0 needs to take into consideration the variation of local incidence angles caused by longer waves on the ocean surface.

Introducing the concept of local incident angle [e.g., *Wright*, 1968; *Valenzuela*, 1978], (1) can be expressed as

$$\Sigma_o(\theta_i) = \frac{|R(0)|^2}{s_f^2} \int \sec^4(\theta_i + \theta) \exp\left(\frac{-\tan^2(\theta_i + \theta)}{s_f^2}\right) p(\theta) d\theta, \quad (3)$$

where θ is the slope of the long wave roughness (the tilting waves) that contributes to the modification of the local incidence angle, $p(\theta)$ is the probability density distribution of the tilting waves, and Σ_0 is the expected radar cross section measured by the altimeter.

For normal incidence, θ_i=0, and (3) becomes

$$\Sigma_o(0) = \frac{|R(0)|^2}{s_f^2} \int \sec^4\theta \exp\left(\frac{-\tan^2\theta}{s_f^2}\right) p(\theta) d\theta. \quad (4)$$

Assuming a normal distribution of the tilting slopes, (4) can be written expressively as

$$\Sigma_o(0) = \frac{|R(0)|^2}{s_f^2} \int \sec^4\theta \exp\left(\frac{-\tan^2\theta}{s_f^2}\right) \frac{1}{\sqrt{2\pi\sigma_t^2}} \exp\left(\frac{-\theta^2}{2\sigma_t^2}\right) d\theta. \quad (5)$$

where σ_t is the RMS value of the tilting surface slopes.

3.2. Wind Speed Algorithm Considering the Surface Tilting Effect

Equation (5) relates the radar backscattering cross section with the mean square surface slopes of both the filtered component and the tilting component. *Hwang* [1997] reviews the optical data of mean square slopes collected in the ocean, which constitute only five data sets (listed in Table 3 and plotted in Figure 6a). Of special interest to this paper are (1) it is concluded that the majority of existing data reflect a linear dependence of the mean square slopes on the wind speed. Some of the data points that deviate from the linear dependence were found to be either under strong swell influence or due to mechanical oscillation of the instrument platform. (2) While the earlier measurements from Sun glitter photography [*Cox and Munk*, 1954] or by single-point laser slope gauges [*Hughes et al.*, 1977; *Tang and Shemdin*, 1983; *Hwang and Shemdin*, 1988] do not provide reliable wavenumber resolution due to the large Doppler frequency shift in the short wave region, the scanning slope sensing data set of *Hwang et al.* [1996] are spatial measurements over a 10-cm segment and sampled at 2-mm intervals. Subsequent data processing using only the central 32 data points (a 6.4 cm coverage) yields the wavenumber spectra in the wavenumber band of 100 to 1600 rad/m. This resolution band is of great interest to radar backscattering using C, X or K band radars. Based on these field measurements (Table 3) of the ocean surface roughness, the total mean square slopes are determined by the combined data sets [*Hwang et al.*, 1997a]:

$$s^2 = 5.12 \times 10^{-3} U_{10} + 1.25 \times 10^{-3}. \quad (6)$$

The filtered mean square slopes for the Ku band altimeter (13.6 GHz) is determined from the wavenumber spectrum obtained by *Hwang et al.* [1996]:

$$s_f^2 = 3.66 \times 10^{-3} U_{10}. \quad (7)$$

The wind-induced component of the tilting mean square slopes for the Ku band altimeter (13.6 GHz) is calculated from the difference of s^2-s_f^2:

$$s_t^2 = 1.09 \times 10^{-3} U_{10} + 1.25 \times 10^{-3}. \quad (8)$$

In addition to the wind-induced tilting slopes, swells and ambient waves caused by other oceanographic processes such as currents and turbulence may introduce additional tilting waves. The total tilting mean square slopes can be expressed as

$$\sigma_t^2 = s_t^2 + S^2. \quad (9)$$

Our knowledge on the quantitative magnitude of the ambient sea surface slopes S^2 is limited. However, given the theoretical limiting steepness of 0.4432 for finite amplitude waves [e.g., *Longuet-Higgins and Fox*, 1978], the upper bound of the mean square slopes of the ambient waves is of the order of $0.4432^2/2 \approx 0.10$. In the Gulf of Mexico, it is found that the value S^2=0.02 gives an overall good fit to the Ku band backscattering cross section. An example is shown in Figure 8, where the data sets A115B220 and A21B220 are used for comparison. The Ku band cross sections are plotted as circles, the computational results using (5) with mean square slope components using (7)-(9) and S^2=0.02 are shown with the solid curves. For a comparison, the results calculated using (2) and (7) are also plotted with the dashed curves, the agreement of the theoretical computation with altimeter measurements is clearly improved with the consideration of local incidence angle modification by surface tilting. Inspecting the curves in Figure 8, it appears that the higher wind cases may have been overcorrected, possibly by the present for-

Table 3. A Description of the Mean Square Slope Data Sets Obtained in the Ocean

Source	Location	Method	Wind Range, m/s
Cox and Munk [1954]	Island of Maui	aerial photography of Sun glitter	0.68 - 13.5
Hughes et al. [1977]	Bute Inlet, Canada	bow-mounted laser slope gauge	3.5 - 7.7
Tang and Shemdin [1983]	North Sea Tower	wave follower laser slope gauge	3.0 - 12.7
Hwang and Shemdin [1988]	Mission Bay Tower, California	wave follower laser slope gauge	2.5 - 6.6
Hwang et al. [1996]	Atlantic Ocean near Gulf Stream	scanning slope sensor buoy	0.47 - 6.0

From *Hwang* [1997].

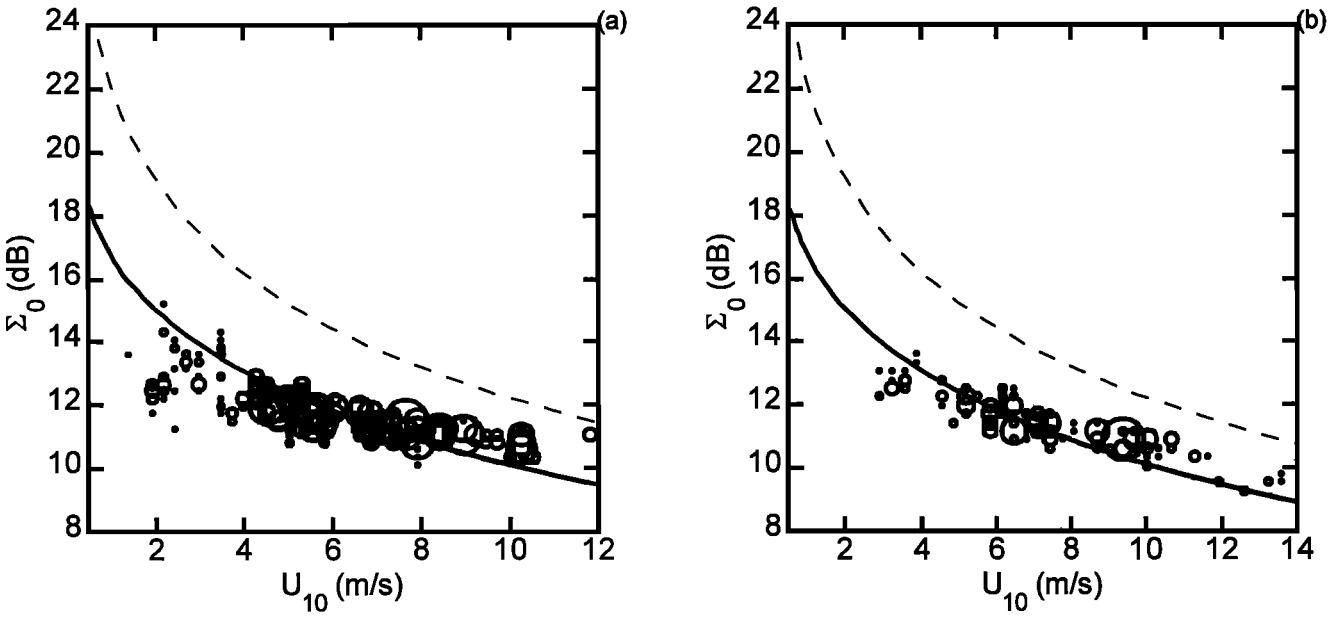

Figure 8. Tilting effect on the altimeter backscattering cross section: (a) data set A115B220, (b) data set A21B220. Circles, TOPEX Ku band measurements; dashed curve, without tilting consideration (equation (2)); solid curve, with tilting effect (equation (5)). The size of the plotting symbol is proportional to the data density.

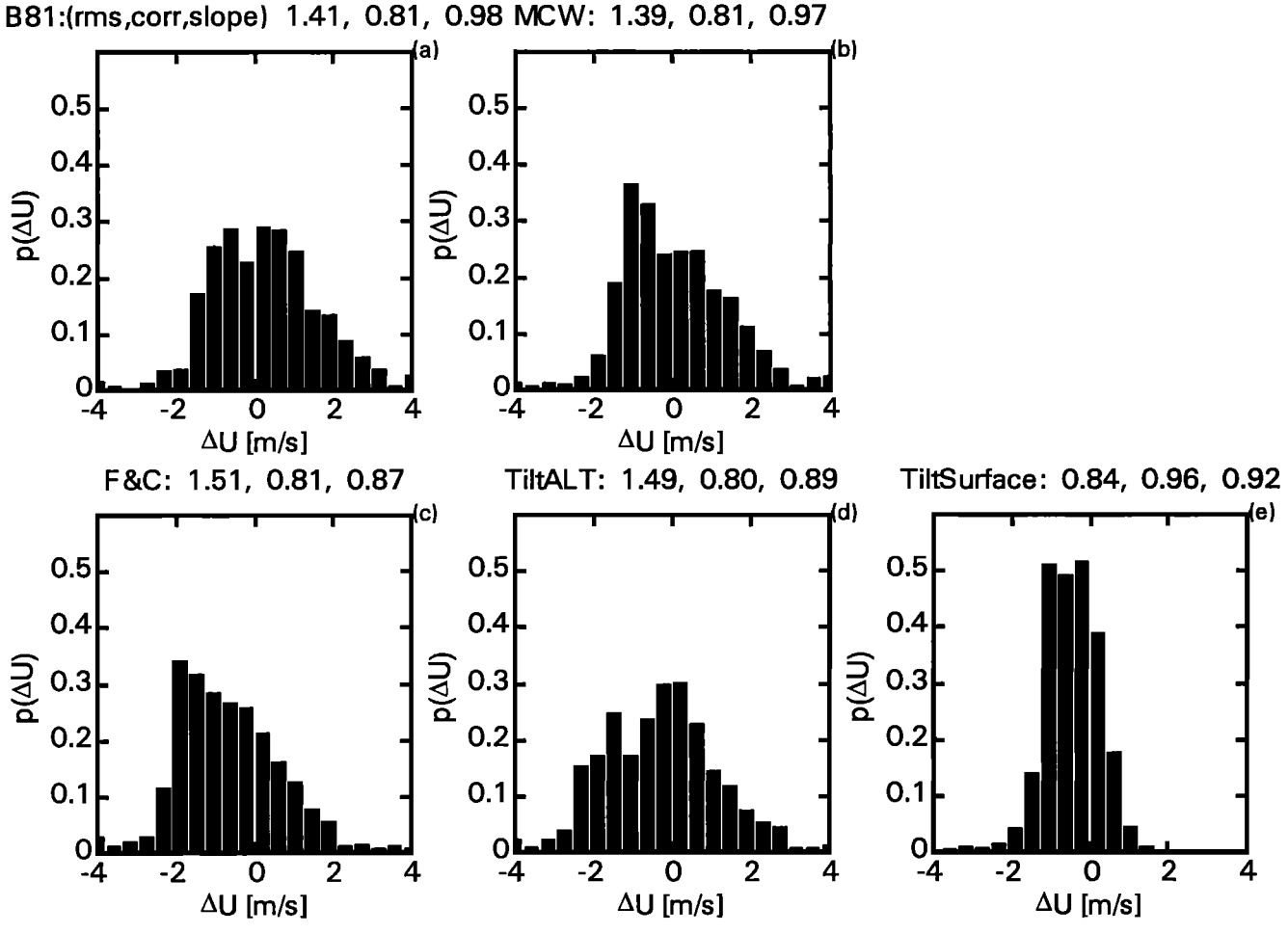

Figure 9. The distributions of wind velocity differences (ALT - Buoy) for the five algorithms discussed in this article. (a) B81 [*Brown et al.*, 1981], (b) MCW [*Witter and Chelton*, 1991], (c) F&C [*Freilich and Challenor*, 1994], (d) Tilt-ALT (equation (11)), and (e) Tilt-Surface (equation (5)).

mulation of a constant S^2. Further improvement can be achieved with a functional form for the ambient mean square slopes. This is not done in this paper due to a lack of information. More detailed discussions of the S^2 parameter are presented by *Hwang et al.* [1997a].

With the assumption of small tilting angles, $\sec^4\theta \approx 1$ and $\tan^2\theta \approx \theta^2$, the integration on the right hand side of (5) can be carried out, the result is

$$\Sigma_o = \frac{|R(0)|^2}{s_f^2}\sqrt{\frac{s_f^2}{s_f^2+2\sigma_t^2}}\,. \tag{10}$$

Substituting $s_f^2=B_1U_{10}$, $s_t^2=B_2U_{10}+B_3$, and $\sigma_t^2=s_t^2+S^2$ (the general forms of (7)-(9)), (10) becomes a quadratic equation of U_{10}, with the following positive root

$$U_{10} = \frac{-K_2+\sqrt{K_2^2+4K_1K_3}}{2K_1}\,, \tag{11}$$

where $K_1=B_1^2+2B_1B_2$, $K_2=2B_1(B_3+S^2)$, and $K_3=(|R(0)|^2/\Sigma_0)^2$. It is clarified here that the closed form solution of (10) is obtained by integrating (5) with the integration limits from $-\infty$ to $+\infty$. This has violated the assumption of small tilting angle made earlier. The algorithm (11), which is obtained from (10) therefore should be considered semiempirical.

For applications to the Ku band (equations 7 and 8), $B_1=3.66\times10^{-3}$, $B_2=1.09\times10^{-3}$, $B_3=1.25\times10^{-3}$, $|R(0)|^2=0.61$, and Σ_0 is the measured Ku band altimeter cross section. The parameter S^2 is empirically determined to be 0.02 for the Gulf of Mexico region. The coefficients for C band are not known because there is a major gap in the wavenumber spectral properties of the ocean surface roughness in the wavelength range between 10 cm and 10 m [*Hwang*, 1997]. This length scale range is very important to the determination of the effective roughness for the C band radar.

Equation (11) can be used to calculate U_{10} from the measured cross section Σ_0. This computation procedure will be called Tilt-ALT in the following comparison. Alternatively, the difference between (10) and (2), denoted $\Delta\sigma_0$, as a function of U_{10} can be calculated as a correction to the cross section measurement. Writing $\sigma_0=\Sigma_0-\Delta\sigma_0$, the wind speed can be obtained from (2) and (7), this calculation will be called Tilt-Surface in the following. The major difference between Tilt-ALT and Tilt-Surface is that the latter procedure assumes a priori knowledge of the tilting surface slopes for computing the tilting correction in the radar cross section. It is found that while the tilting correction, $\Delta\sigma_0$, or correspondingly the tilting slope, is a monotonic function of the wind speed, the dependence on the measured cross section is not monotonic [*Hwang et al.*, 1997a]. Being able to apply an accurate correction $\Delta\sigma_0$ to the altimeter cross section, the retrieved wind speed is also much more accurate in the Tilt-Surface procedure, as shown by *Hwang et al.* [1997a] using data set T115B220. More extensive comparison will be presented in the next section.

3.3. Comparison With Buoy Measurements

Figure 9 shows the distributions of the wind speed difference, ΔU (altimeter-buoy), between in situ buoy data and altimeter

Table 4. Comparison Statistics of Five Wind Speed Algorithms

	B81	MCW	F&C	Tilt-ALT	Tilt-Surface
		RMS σ_U, m/s			
A115B220	1.41	1.39	1.51	1.49	0.84
A21B220	1.28	1.35	1.62	1.58	0.97
A46B203	1.75	1.74	1.79	1.83	1.07
A59B202	1.30	1.14	1.33	1.56	0.86
A46B236	1.30	1.36	1.46	1.41	0.80
A26B202	2.73	1.45	1.52	1.65	1.21
A26B235	1.54	1.71	1.92	1.66	1.09
		Correlation Coefficient, R			
A115B220	0.81	0.81	0.81	0.80	0.96
A21B220	0.90	0.90	0.90	0.89	0.97
A46B203	0.82	0.83	0.83	0.81	0.95
A59B202	0.92	0.93	0.93	0.91	0.98
A46B236	0.90	0.91	0.91	0.90	0.98
A26B202	0.65	0.88	0.87	0.80	0.91
A26B235	0.81	0.82	0.82	0.81	0.95
		Bias, m/s			
A115B220	0.23	0.04	-0.06	-0.31	0.12
A21B220	-0.28	-0.31	-0.98	-0.86	-0.21
A46B203	0.25	0.03	-0.59	-0.25	0.11
A59B202	-0.01	-0.07	-0.73	-0.59	-0.04
A46B236	0.13	-0.18	-0.72	-0.35	0.04
A26B202	0.42	0.17	-0.48	-0.25	0.21
A26B235	-0.20	-0.59	-1.16	-0.66	-0.20
		Slope0			
A115B220	0.98 (1.00)	0.97 (1.00)	0.87 (0.89)	0.89 (0.92)	0.98 (0.99)
A21B220	0.93 (0.95)	0.96 (097)	0.87 (0.89)	0.85 (0.86)	0.95 (0.96)
A46B203	0.96 (0.99)	0.96 (1.00)	0.87 (0.90)	0.88 (0.91)	0.97 (0.98)
A59B202	0.95 (0.96)	0.97 (0.98)	0.89 (0.90)	0.86 (0.88)	0.96 (0.97)
A46B236	0.97 (0.99)	0.97 (0.99)	0.88 (0.91)	0.89 (0.91)	0.98 (0.99)
A26B202	1.04 (1.11)	1.02 (1.04)	0.93 (0.95)	0.93 (0.95)	1.01 (1.03)
A26B235	0.92 (0.95)	0.89 (0.92)	0.80 (0.83)	0.85 (0.87)	0.94 (0.95)

measurements based on five different algorithms: B81 [*Brown et al.*, 1981], modified Chelton and Wentz (MCW) [*Witter and Chelton*, 1991], Freilich and Challenor (hereinafter referred to as F&C) [*Freilich and Challenor*, 1994]; Tilt-ALT, Equation (11); and Tilt-Surface, the forward computation procedure described in the last section. The distributions of the first three empirical algorithms (Figures 9a-9c) are quite similar, as had been illustrated in previous comparisons [e.g., *Witter and Chelton*, 1991; *Wu*, 1992; *Freilich and Challenor*, 1994] and commented on in section 3.1. The RMS difference and the correlation coefficient are (1.41 m/s, 0.81), (1.39 m/s, 0.81), and (1.51 m/s, 0.81) for B81, MCW, and F&C, respectively. The consideration of the tilting surface effect results in two different algorithms described in the last section. The statistical properties of the wind speed difference based on the operational algorithm (Tilt-ALT) are very similar to the other three algorithms just discussed (Figure 9d), the RMS difference and the correlation coefficient are (1.49 m/s, 0.80). However, if the tilting slope can be accurately calculated, and the correction to the measured cross section applied properly, the distribution of wind speed difference is noticeably narrowed (Figure 9e), the RMS difference and the correlation coefficient improve significantly to (0.84 m/s, 0.96). Similar improvements are found with other data sets. Table 4 lists the RMS difference, correlation coefficient, bias, and *slope0* of the surface wind speed comparisons using the five algorithms just described and applied to all the Gulf of Mexico data sets listed in Table 1. We may conclude from this comparison that the accuracy of the satellite altimeter is considerably better than we have previously accepted. If independent measurement of the tilting slope is available, for determining the coefficients B_2, B_3, and S^2 in (11), the RMS difference between the altimeter output and in situ measurements will reduce from the currently accepted magnitudes established by empirical algorithms. The improvement is approximately 40% based on the results shown in Table 4. And most significant of all, this conclusion is based on sound physical ground relating the altimeter backscattering and the surface slope properties, unlike the earlier operational algorithms that depend on empirical formulae established from collocated buoy and altimeter databases.

3.4. Spatial and Temporal Lags

The effect of spatial and temporal lags on the wind speed comparison is investigated using a similar procedure for studying the influence of spatial and temporal lags on the altimeter and buoy wave height comparison (section 2.2). The results in terms of the RMS difference and the correlation coefficient are shown in Figure 10 for data set A115B220 and in Figure 11 for data set A21B220. Similar to the results of the significant wave height, reducing the spatial lag persistently improves the agreement of wind speed measurements from the altimeter and ocean buoys. Computations from two operational algorithms (MCW and B81) indicate identical trends of decreasing correlation coefficient from approximately 0.86 at 8 km lag to 0.72 at 48 km lag (data set A115B220, Figure 10a). The corresponding RMS difference increase from 1.3 to 1.6 m/s (Figure 10b). The correlation coefficients calculated for the data set A21B220 are higher than those of the data set A115B220 (compare Figures 10a and 11a), but the RMS differences as a function of space lags are similar (compare Figures 10b and 11b). Of the four operational algorithms studied (B81, MCW, F&C, and Tilt-ALT), MCW produces better results in general than the other three. The differences among these operational algorithms are relatively minor compared to the performance of the Tilt-Surface algorithm. The correlation coefficients of the latter exceed 0.95 and the RMS differences are less than 1.0 m/s when the spatial lags are less than 30 km (Figures 10a, 10b, 11a, and 11b). These results again strongly suggest that the wind speed accuracy derived from the satellite altimeter is much better than previously reported.

4. Wave Period

4.1. Dimensionless Wave Parameters

It is generally recognized that in a wind-generated ocean wave system, there is a close correlation among the three key parameters of the wave field: wind speed, wave height, and wave period. Such correlation had been established through theoretical analysis of wave dynamics and confirmed with ocean wave measure-

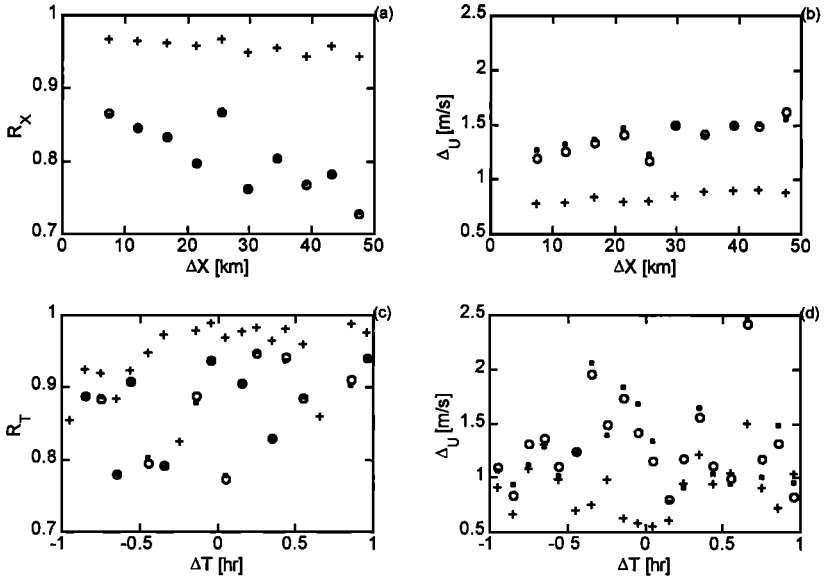

Figure 10. The correlation coefficient and RMS difference of wind speed measurements as functions of (a, b) space lags and (c, d) time lags, data set A115B220. Crosses, B81 [*Brown et al.*, 1981], open circles, MCW [*Witter and Chelton*, 1991], and pluses, Tilt-Surface (equation (5)).

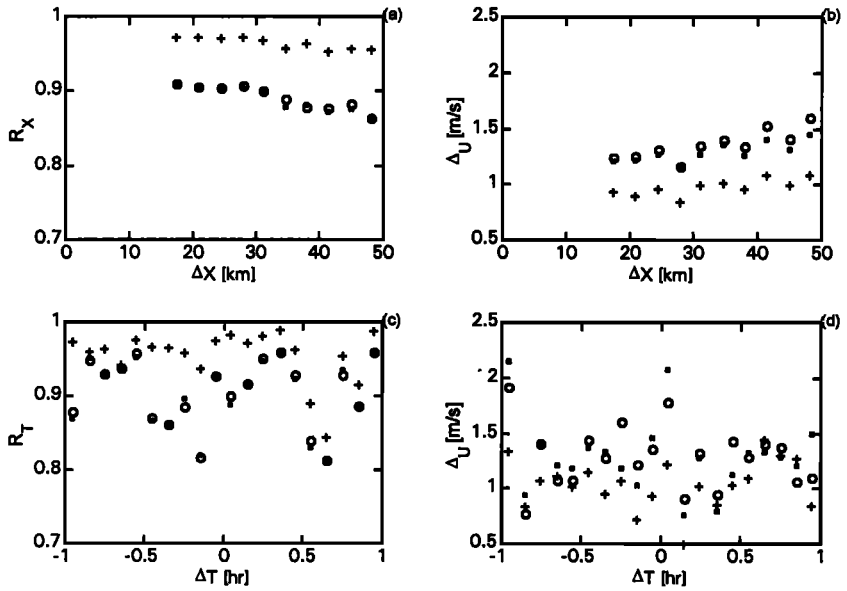

Figure 11. The correlation coefficient and RMS difference of wind speed measurements as functions of (a, b) space lags and (c, d) time lags, data set A21B220. Crosses, B81 [*Brown et al.*, 1981], open circles, MCW [*Witter and Chelton*, 1991], and pluses, Tilt-Surface (equation (5)).

ments [e.g., *Hasselmann et al.*, 1973, 1976; *Toba*, 1978]. *Hasselmann et al.* [1973, 1976] discuss the fetch dependence of one-dimensional spectra and establish the three key dimensionless wave parameters, the peak frequency $f_m^*=f_m U_{10}/g$, the fetch $x^*=xg/U_{10}^2$, and the total wave energy $E^*=g^2E/U_{10}^4$, where the asterisk denotes the dimensionless parameters and g is the gravitational acceleration. They show that the three parameters are closely related by the following equations:

$$f_m^* = 3.5x^{*-0.33}, \tag{12}$$

$$E^* = 1.6\times 10^{-7} x^* . \tag{13}$$

The linear equation (13) can be substituted into (12) to derive the functional relationship of the wave frequency, wind speed, and wave energy and eliminate the fetch parameter. The formula relating the three parameters, wind speed (U_{10}), wave height (H), and the characteristic wave period (T) can be derived using the relations $E=\eta_{RMS}^2$, $H=4\eta_{RMS}$, and the inverse relation of wave period and wave frequency. The quantity η_{RMS} is the root mean square of the sea surface displacement. In the original derivation the peak wave period T_p of the wave spectrum was used as the

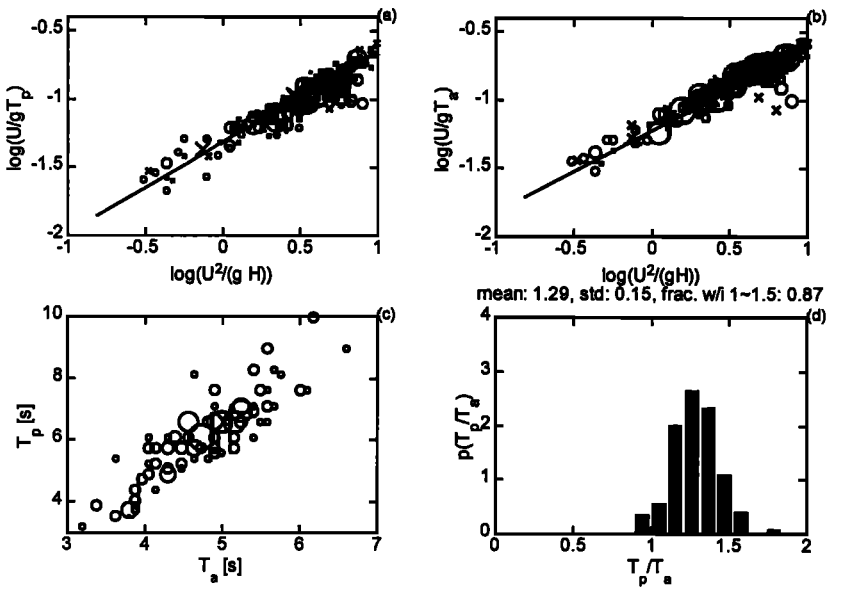

Figure 12. (a) (U_{10}/gT_p) versus (U_{10}^2/gH), solid curve is equation (14) [*Hasselmann et al.*, 1973, 1976]; (b) (U_{10}/gT_a) versus (U_{10}^2/gH), solid curve is equation (15) [*Toba*, 1978]. Symbols used are open circles, time lag group 1 and crosses, time lag group 2, (c) buoy-measured T_p versus T_a, and (d) the distribution of the ratio T_p/T_a. Date set T115B220. The size of the plotting symbol is proportional to the data density.

characteristic wave period based on several groups of experimental data. The resulting equation is

$$\frac{U_{10}}{gT_p} = 4.8\times10^{-2}\left(\frac{U_{10}^2}{gH}\right)^{2/3}. \quad (14)$$

The tight correlation between U_{10}/gT_p and U_{10}^2/gH is also found in the Gulf of Mexico wave data (Figure 12a). The bias and the symmetric regression coefficient [*Bauer et al.*, 1992] for the fitting are 0.006 and 1.05 for the time lag group 1 data respectively, and 0.002 and 1.00 for the time lag group 2 data. The correlation function was established based on a "saturated" sea condition that characterizes the local wind-generated wave system. When swells from distant wind sources are present, the correlation needs to be modified. The Gulf of Mexico, being a semienclosed sea, is found to be less dominated by long swell systems. From experience of analyzing the Gulf of Mexico wave data, it is found that the wave energy associated with the swell frequency rarely exceeds 15% of the total spectral energy in the region. Although we have not tested this procedure to calculate the wave frequency from altimeter data in other regions of the world, it is noticed that (14) is a very robust equation relating the wave period to the wind speed and wave height. The effect of swells will modify mainly the significant wave height derived by the sensor. Because the wave period is related to the wave height as $T\sim H^{2/3}$ (14), the error introduced by swell presence can be quantified. For example, if the spectral intensity in the swell-sea system doubles by the presence of swells, the wave height of the saturated sea will be overestimated by a factor of $2^{1/2}$, and introduce an overestimation of wave period by approximately 25%.

4.2. Characteristic Wave Period

Based on the experience from analyzing the wave spectrum it is found that the peak wave period is an unstable quantity and may show a large variation when different data processing procedures are used. Alternatively, the average wave period T_a, can be used in place of the peak wave period. (T_a is defined here as $[\int f^2 S(f)df / \int S(f)df)]^{-1/2}$, where f is the wave frequency and $S(f)$ is the frequency spectrum.) Because T_a is an integrated property, it is more robust than T_p. Both T_p and T_a are standard output of the NDBC buoy data set. Figure 12b shows U_{10}/gT_a versus U_{10}^2/gH, indicating a comparable tight grouping of the two dimensionless parameters as those in Figure 12a. The trend is slightly different from (14). Empirically, the following equation provides a good agreement with the buoy measurements in the Gulf of Mexico,

$$\frac{U_{10}}{gT_a} = 6.0\times10^{-2}\left(\frac{U_{10}^2}{gH}\right)^{0.6}. \quad (15)$$

The bias and the symmetric regression coefficient [*Bauer et al.*, 1992] are –0.008 and 0.94 for the group 1 data and –0.012 and 0.91 for the group 2 data, respectively. Equation (15) is in excellent agreement with *Toba*'s [1978] power law relation between the dimensionless significant wave height and wave period for growing wind waves.

The ratio of T_p/T_a tends to be rather constant as shown in Figures 12c and 12d. The average ratio with 1 standard deviation is 1.29 ± 0.14. In either case of using T_p or T_a as the characteristic wave period, the data points collapse together and follow the functional forms suggested by (14) and (15) very well (Figures 12a and 12b). It is therefore expected that using the TOPEX altimeter output, the characteristic wave period of the wave field can be derived using either (14) for the peak period or (15) for the average period.

4.3. Characteristic Wave Period From Altimeter

From the above discussion, it is conceivable that the altimeter data can also provide the characteristic period of a wave field. It

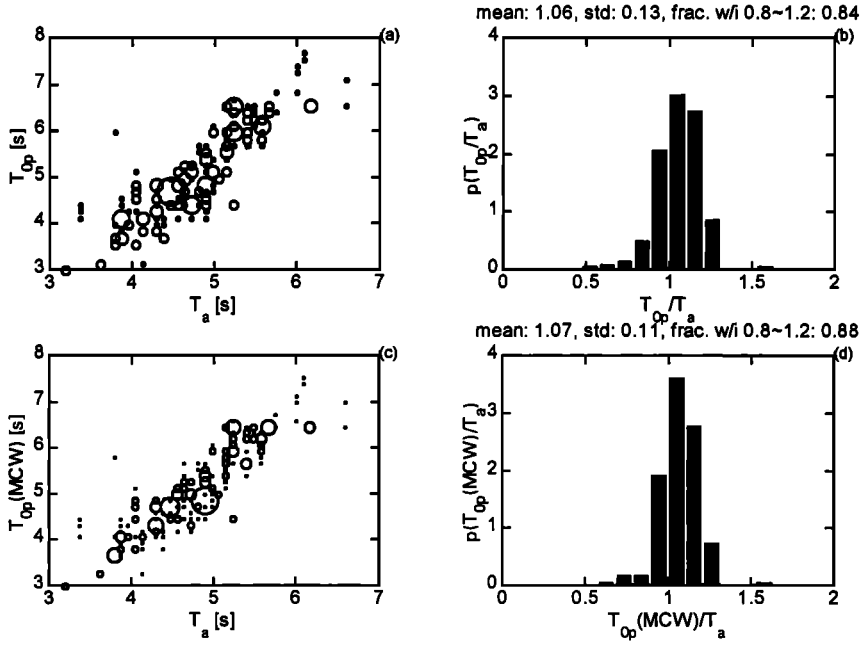

Figure 13. (a) The characteristic (peak) wave period T_{0p} derived from TOPEX Ku band output of wind speed and wave height, plotted against T_a. (b) The distribution of the ratio T_{0p}/T_a. Tilt-Surface wind speed algorithm is used in the above computation. (c, d) Same as Figures 13a and 13b but the MCW algorithm was used to derive the wind speed from the satellite altimeter cross section. Data set T115B220. The size of the plotting symbol is proportional to the data density.

has been established in sections 2 and 3 that the precision of wind speed and wave height measurements from the altimeter is quite high, we expect that the wave period derived from the TOPEX output will be also comparable to the measurement from in situ buoys. Figure 13a shows the characteristic (peak) wave period T_{0p} calculated from (14) using the altimeter-derived wind speed (Tilt-Surface procedure, the optimal accuracy calculation) and wave height, plotted against the buoy-measured average period. The appearance of a large data scatter is due partially to the coarse digitization - buoy output of the wave period is in 0.1 s unit. The 1331 data pairs of buoy-measured T_p and T_a result in less than 80 discrete pairs. Figure 12c uses different symbol sizes to denote the data density. The distribution of T_{0p}/T_a is shown in Figure 13b, which is very similar to the distribution of T_p/T_a (Figure 12d). The average ratio of T_{0p}/T_a with 1 standard deviation is 1.21±0.15, slightly less than that of T_p/T_a (1.29±0.14) and with a similar data spread. The distribution of both ratios, T_p/T_a and T_{0p}/T_a, are very narrow (Figures 12d and 13b), the fraction falling within the range of 1 to 1.5 is 0.89 for the former and 0.90 for the latter. These statistics are very similar for the other data sets also, the results are given in Table 5.

We also applied the calculation procedure using the wind speed derived from the operational algorithms. The results are not significantly different from those using the Tilt-Surface derived wind speed. An example is shown in Figures 13c and 13d for the computational results using the MCW wind speed. The degree of data scatter in the T_{0p} versus T_p plot, and the distribution of the T_{0p}/T_a ratio are quite similar to the buoy measured results. For the case in this illustration, the mean value of T_{0p}/T_a with 1 standard deviation is 1.23±0.15, and the fraction of the ratio falling between 1 and 1.5 is 0.88. A similar level of agreement is found when using (15) to calculate the average wave period (T_{0a}) from the altimeter output. The ratio of the average period from the two sensing systems (altimeter and buoy) with 1 standard deviation for each data set is listed in Table 5 also.

It is concluded that one can derive the characteristic wave period from satellite altimeters. Using (14), the average ratio of the normalized period, T_{0p}/T_a, is approximately 4% less than that of T_p/T_a of the buoy measurements, and the scattering of the ratio T_{0p}/T_a is somewhat larger than the corresponding buoy measurements of T_p/T_a. The distributions of the two ratios are quite similar in the statistical sense.

Concluding the results of sections 2, 3, and 4, the three most important properties of a wave field, the significant wave height, significant wave period and wind speed, can be derived from satellite altimeters. Figures 14a, 14b, and 14c display the comparisons of the significant wave height, wind speed and characteristic (average) wave period derived from the TOPEX Ku band altimeter and NDBC buoy. Only data points within 10 km spatial lags are used (data set T115B220). The measurements from the two systems are essentially equivalent. The average ratio with 1 standard deviation of the wave heights, wind speeds, and characteristic wave periods are 1.01±0.14, 0.95±0.11, and 1.06±0.13, respectively. The distributions of these ratios are shown in Figures 14d, 14e, and 14f, showing very narrow spreading.

5. Summary

In this article we have presented comparisons of altimeter-derived wave height, wind speed and wave period with corresponding measurements from NDBC buoys in the Gulf of Mexico. The closest distance of the buoy location to the TOPEX track is less than 6 km (A115B220). The quantitative effect of the spatial lag on the correlation of the TOPEX altimeter and surface buoy measurements of wind and wave parameters is studied, using the long time series available (3.15 years used in this study) for building up sufficient statistical confidence. In a similar fashion, the effect of temporal lag between altimeter and buoy measurements is also investigated. It is found that the agreement between altimeter and buoy measurements of wind speed and wave height improve with shorter spatial lags, while time lags of up to 1 hour do not produce significant changes in the key statistics such as the RMS difference and the correlation coefficient. For future calibration purposes, it is then more critical to select in situ measurements that are closer to the satellite tracks while the temporal lag can be relaxed.

In the course of studying the wind speed derivation from satellite altimeters, it is found that the surface tilting effect is a significant factor of consideration. The effect is especially noticeable at lower wind velocities where differences of more than 6 dB are found between the altimeter measurements and the computations using the classical equation relating the backscattering cross section and the surface roughness (e.g., equation (2)). With the correction of the tilting effect in the cross section measurement, the calculated wind speed is found to be in much better agreement with the surface buoy measurement. The improvement is of the order of 40% when compared to the results derived from other statistical or empirical algorithms including *Brown et al.* [1981], *Witter and Chelton* [1991], and *Freilich and Challenor* [1994]. This result suggests that the theoretical framework relating the backscattering cross section and the surface roughness is fundamentally sound when the tilting effect that modifies the local incident angle is taken into account. It also indicates that the accuracy of deriving wind speeds from altimeter cross sections is

Table 5. Comparison of Characteristic Period Derived From Altimeters and Buoys

	T_p/T_a,	T_{0p}/T_a,	Fraction Between 1 and 1.5		T_{0d}/T_a Tilt-Surface,	T_{0d}/T_a MCM,
	mean ± 1 std	mean ± 1 std	T_p/T_a	T_{0p}/T_a	mean ± 1 std	mean ± 1 std
A115B220	1.29±0.14	1.21±0.15	0.89	0.90	1.06 ± 0.13	1.07 ± 0.11
A21B220	1.29±0.15	1.26±0.23	0.82	0.86	1.09 ± 0.15	1.10 ± 0.13
A46B203	1.26±0.20	1.21±0.28	0.70	0.84	1.03 ± 0.20	1.04 ± 0.19
A59B202	1.27±0.14	1.23±0.25	0.85	0.95	1.06 ± 0.16	1.07 ± 0.15
A46B236	1.21±0.20	1.18±0.31	0.79	0.79	1.00 ± 0.18	1.03 ± 0.17
A26B202	1.26±0.15	1.20±0.23	0.81	0.89	1.04 ± 0.16	1.05 ± 0.15

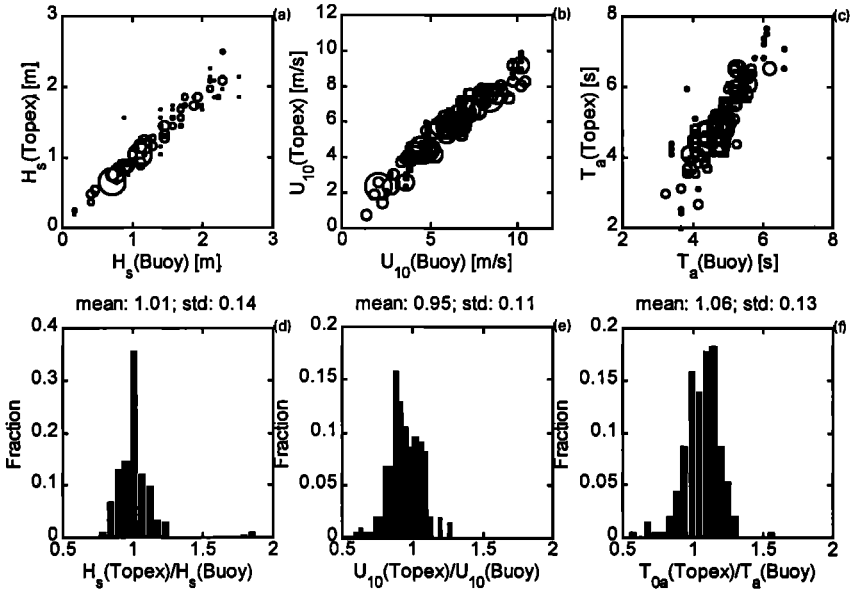

Figure 14. Comparison of the altimeter and buoy measurements of the (a) significant wave height, (b) wind speed, and (c) characteristic (average) wave period. Only data points with spatial lags less than 10 km are included in this comparison. (d, e, f) The ratios (TOPEX measurements divided by buoy measurements) of these three wave parameters. Data set T115B220. The size of the plotting symbol is proportional to the data density.

potentially much better than we have perceived, however, in order to achieve the full potential of the altimeter wind sensing, independent measurement of the sea surface slope component contributing to the tilting may be needed.

The statistics of comparison indicate that the agreement of wave height measurements from TOPEX and ocean buoys is within 0.1 m for the conditions that the separations between the buoy location and altimeter footprints are less than 10 km and the measurement time lags less than 1 hour. This observation is consistent with that reported by *Gower* [1996], who has found that the RMS scatter for separations less than 10 km is between 0.14 and 0.15 m [*Gower*, 1996, Table 4]. The larger scatter is mainly due to the small sample populations, which are less than 30 for the 10-km subsets in Gower's study. These RMS scatters are considerably less than the numbers specified by *Monaldo* [1988], who has estimated that the RMS uncertainty due to sampling variability from the buoy alone is 0.24 m. Despite these quantitative differences, *Monaldo* [1988] estimates that the error due to spatial proximity (of 50 km maximal distance) is about 3 times larger than the error due to the temporal differences (of 1 hour). Our results on the spatial and temporal decorrelation analyses are in agreement with this assessment. For wind speeds derived from the empirical algorithms, the comparisons using the Gulf of Mexico data are also statistically similar to the results reported by *Gower* [1996], which are very close to the estimates of *Monaldo* [1988].

Our study also indicates that the characteristic wave period can be obtained from altimeter output, at least for enclosed seas such as the Gulf of Mexico where swell systems from distance sources are not prominent. Errors due to the swell effect when applying the present procedure can be estimated as described in section 4.1. Such capability to accurately monitor the global ocean waves from space is very significant for scientific research and engineering applications related to ocean waves.

Appendix: Regression Coefficients

When the intercept is forced to zero, the linear fitting of the two variables represents the proportionality of the two quantities, which can be written as

$$y_i = cx_i, \tag{A1}$$

where (x_i, y_i), i=1, 2, ... N are the N data pairs subject to the statistical analysis, and c is the proportionality coefficient. There are a few different ways of deriving the proportionality coefficient [*Bauer et al.*, 1992; *Romeiser*, 1993]. Minimizing the mean square error in the y direction yields the regression coefficient

$$c_y = \frac{\langle xy \rangle}{\langle x^2 \rangle}, \tag{A2}$$

where the angle brackets represent the ensemble average of the quantities inside the brackets. Alternatively, minimizing the mean square error in the x direction, $\langle (y - c_x x)^2 \rangle$, yields

$$c_x = \frac{\langle y^2 \rangle}{\langle xy \rangle}. \tag{A3}$$

Since

$$\frac{c_y}{c_x} = \frac{\langle xy \rangle^2}{\langle x^2 \rangle \langle y^2 \rangle} = r^2 \le 1, \tag{A4}$$

where r is the correlation coefficient, $c_y \le c_x$ is always satisfied. The regression coefficients c_x and c_y are obviously asymmetric with an asymmetric bias. In general, the two sets of quantities for the statistical analysis are both subject to measurement errors. Frequently, one of the two sets has a better defined error statistics and can be used as the preferred reference. Sometimes the error statistics of the two sets are about equal, and neither is the pre-

ferred reference. The wave height measured by ocean buoys and spaceborne altimeters fall into the latter category. The buoy measurements are in situ, yet the sensors and platforms are subject to the harsh oceanic environment. The spaceborne altimeter measurements are indirect but from a stable platform that is outside of the atmospheric and oceanic disturbances. Two symmetric regression coefficients that are invariant with respect to the interchange of x and y are defined by *Bauer et al.* [1992]

$$c = (c_x c_y)^{1/2} = \left(\frac{\langle y^2 \rangle}{\langle x^2 \rangle}\right)^{1/2}, \quad \text{(A5)}$$

and

$$c' = \tan\left[\frac{1}{2}\tan^{-1}\left(\frac{\langle 2xy \rangle}{\langle x^2 \rangle - \langle y^2 \rangle}\right)\right]. \quad \text{(A6)}$$

Equation (A6) is invariant with respect to the rotations in the xy plane and corresponds to minimizing the orthogonal distances between the data points to the regression line. The coefficient c', however, is found to be very sensitive when the correlation coefficient is close to unity. This is due to the difference term in the denominator of the argument in (A6), as $x \cong y$, the sign of c' can easily change. Also, the regression coefficient computed using (A5) is always positive, which may be erroneous. These shortcomings can be rectified by preserving the sign of the slope of the scatterplot, that is, rewrite the last two equations as

$$c = \mathrm{sgn}(\langle xy \rangle)(c_x c_y)^{1/2} = \mathrm{sgn}(\langle xy \rangle)\left(\frac{\langle y^2 \rangle}{\langle x^2 \rangle}\right)^{1/2}, \quad \text{(A5')}$$

where sgn is the signum function , and

$$c' = \begin{cases} \tan\left\{\frac{1}{2}\tan^{-1}\left(\frac{\langle 2xy \rangle}{\langle x^2 \rangle - \langle y^2 \rangle}\right)\right\} & \langle x^2 \rangle \geq \langle y^2 \rangle \\ \tan\left\{\frac{1}{2}\left[\tan^{-1}\left(\frac{\langle 2xy \rangle}{\langle x^2 \rangle - \langle y^2 \rangle}\right) + \pi\right]\right\} & \langle x^2 \rangle < \langle y^2 \rangle \end{cases} \quad \text{(A6')}$$

Alternatively, using the sign of coefficient c_y, the coefficients c and c' can be expressed as $\mathrm{sgn}(c_y)|c|$ and $\mathrm{sgn}(c_y)|c'|$, respectively, where c and c' in the absolute sign are calculated by (A5) and (A6).

Both *Bauer et al.* [1992] and *Romeiser* [1993] use the coefficient c in (A5) for the symmetrical regression coefficient for their statistical discussions. The coefficient c is also used in this paper as listed in Tables 2 and 4 in parentheses. The coefficients c, c', c_x, and c_y become indistinguishable as the correlation coefficient r approaches unity.

Acknowledgments. This work is sponsored by the Office of Naval Research, Naval Research Laboratory Job Orders 73-6800-07, 73-7046-07, and 73-7075-06 and National Data Buoy Center, contract XA2310501. The authors would like to acknowledge the careful review and many constructive comments from Jacqueline Boutin, Brian Sanderson, and an anonymous reviewer. NRL contribution JA--7332-97-0011.

References

Barrick, D. E., Rough surface scattering based on the specular point theory, IEEE *Trans. Antennas Propag., AP-16*, 449-454, 1968.

Bauer, E., S. Hasselmann, and K. Hasselmann, Validation and assimilation of Seasat altimeter wave heights using the WAM wave model, *J. Geophys. Res., 97*, 12671-12682, 1992.

Brown, G. S., Backscattering from a Gaussian-distributed perfectly conducting rough surface, *IEEE Trans. Antennas Propag., AP-26*, 472-482, 1978.

Brown, G. S., Quasi-specular scattering from the air-sea interface, in *Surface Waves and Fluxes*, vol. 2, edited by W. Plant and G. Geernaert, pp. 1-40, Kluwer Acad., Norwell, Mass., 1990.

Brown, G. S., H. R. Stanley, and N. A. Roy, The wind speed measurement capability of spaceborne radar altimeters, *IEEE J. Oceanic Eng., OE-6*, 59-63, 1981.

Chelton, D. B., and F. J. Wentz, Further development of an improved altimeter wind speed algorithm, *J. Geophys. Res., 91*, 14250-14260, 1986.

Chelton, D. B., E. J. Walsh, and J. L. MacArther, Pulse compression and sea level tracking in satellite altimetry, *J. Atmos. and Oceanic Technol., 6*, 407-438, 1989.

Cox, C. S., and W. Munk, Statistics of the sea surface derived from Sun glitter, *J. Mar. Res., 13*, 198-227, 1954.

Ebuchi, N., and H. Kawamura, Validation of wind speeds and significant wave heights observed by the TOPEX altimeter around Japan, *J. Oceanogr., 50*, 479-487, 1994.

Freilich, M. H., and P. G. Challenor, A new approach for determining fully empirical altimeter wind speed model functions, *J. Geophys. Res., 99*, 25051-25062, 1994.

Fu, L.-L., E. J. Christensen, and C. A. Yamarone, TOPEX /POSEIDON mission overview, *J. Geophys. Res., 99*, 24369-24381, 1994.

Gower, J. F. R., Intercomparison of wave and wind data from TOPEX/POSEIDON, *J. Geophys. Res., 101*, 3817-3829, 1996.

Hasselmann, K. et al., Measurements of wind-wave growth and swell decay during the Joint North Sea Wave Project (JONSWAP), Erganzungsheft zur Dtsch. Hydrogr. Z., *Reihe A(8), Nr. 12*, 95 pp, Dtsch. Hydrogr. Inst., Hamburg, Germany, 1973.

Hasselmann, K., D. B. Ross, P. Miller, and W. Sell, A parametric wave prediction model, *J. Phys. Oceanogr., 6*, 200-228, 1976.

Hughes, B. A., H. L. Grant, and R. W. Chappell, A fast response surface wave slope meter and measured wind-wave moment, *Deep Sea Res., 24*, 1211-1223, 1977.

Hwang, P. A., A study of the wavenumber spectra of short water waves in the ocean, 2, Spectral model and mean square slope, *J. Atmos. Oceanic Technol., 14*, 1174-1186, 1997.

Hwang, P. A., and O. H. Shemdin, The dependence of sea surface slope on atmospheric stability and swell condition, *J. Geophys. Res., 93*, 13903-13912, 1988.

Hwang, P. A., S. Atakturk, M. A. Sletten, and D. B. Trizna, A study of the wavenumber spectra of short water waves in the ocean, *J. Phys. Oceanogr., 26*, 1266-1285, 1996.

Hwang, P. A., D. W. Wang, W. J. Teague, and G. A. Jacobs, Effect of surface tilting on altimeter wind measurement, *Nav. Res. Lab. Memo. Rep. NRL/MR/7332-97-8067*, 19 pp., Nav. Res. Lab., Stennis Space Center, MS, 1997a.

Hwang, P. A., W. J. Teague, G. A. Jacobs, and D. W. Wang, Measurement of wind and wave parameters from satellite altimeters, *Proc. 4th Int. Conf. Remote Sens. Mar. Coastal Env., 1*, 441-450, 1997b.

Jackson, F. C., W. T. Walton, D. E. Hines, B. A. Walter, and C. Y. Peng, Sea surface mean square slope from Ku-band backscatter data, *J. Geophys. Res., 97*, 11411-11427, 1992.

Liu, W. T., K. B. Katsaros, and J. A. Businger, Bulk parameterization of air-sea exchanges of heat and water vapor including the molecular constraints at the interface, *J. Atmos. Sci., 36*, 1722-1735, 1979.

Longuet-Higgins, M. S., and M. J. H. Fox, Theory of the almost-highest waves, 2, Matching and analytical extension, *J. Fluid Mech., 85*, 769-786, 1978.

Monaldo, F., Expected differences between buoy and radar altimeter estimates of wind speed and significant wave height and their implications on buoy-altimeter comparisons, *J. Geophys. Res., 93*, 2285-2302, 1988.

Romeiser, R., Global validation of the wave model WAM over a 1-year period using Geosat wave height data, *J. Geophys. Res., 98*, 4713-4726, 1993.

Tang, S., and O. H. Shemdin, Measurement of high-frequency waves using a wave follower, *J. Geophys. Res.*, *88*, 4832-4840, 1983.

Teague, W. J., P. A. Hwang, D. W. Wang, G. A. Jacobs, A three-year climatology of waves and winds in the Gulf of Mexico, *Nav. Res. Lab. Memo. Rep. NRL/MR/7332-97-8068*, 20 pp., Nav. Res. Lab., Stennis Space Center, MS, 1997.

Toba, Y., Stochastic form of the growth of wind waves in a single-parameter representation with physical interpretation, *J. Phys. Oceanogr.*, *8*, 494-507, 1978.

Valenzuela, G. R., Theories for the interaction of electromagnetic and oceanic waves: A review, *Boundary Layer Meteorol.*, *13*, 61-85, 1978.

Witter, D. L., and D. B. Chelton, A Geosat altimeter wind speed algorithm and a method for altimeter wind speed algorithm development, *J. Geophys. Res.*, *96*, 8853-8860, 1991.

Wright, J. W., A new model for sea clutter, *IEEE Trans. Antennas Propag.*, *AP-16*, 217-223, 1968.

Wu, J., Near-nadir microwave specular returns from the sea surface - altimeter algorithm for wind and wind stress, *J. Atmos. Oceanic Technol.*, *9*, 659-667, 1992.

P.A. Hwang, G. A. Jacobs, and W. J. Teague, Code 7300, Oceanography Division, Naval Research Laboratory, Stennis Space Center, MS 39529-5004. (e-mail: paul.hwang@nrlssc.navy.mil, jacobs@nrlssc.navy.mil, teague@nrlssc.navy.mil)

D. W. Wang, Computer Science Corp., Stennis Space Center, MS 39529-5004. (e-mail: dwang@tsc.ndbc.noaa.gov)

(Received April 7, 1997; revised December 29, 1997; accepted January 16, 1998.)